Passive temperature tomography experiments to characterize transmissivity and connectivity of preferential flow paths in fractured media

Maria Klepikova, Tanguy Le Borgne, Olivier Bour, Kerry Gallagher, Rebecca Hochreutener, Nicolas Lavenant

▶ To cite this version:

[1] # Passive temperature tomography experiments to
[2] # characterize transmissivity and connectivity of
[3] # preferential flow paths in fractured media

[4] Maria V. Klepikova[a,b,*], Tanguy Le Borgne[a], Olivier Bour[a], Kerry
[5] Gallagher[a], Rebecca Hochreutener[a], Nicolas Lavenant[a]

[6] [a]*Géosciences Rennes, OSUR, UMR CNRS 6118, University of Rennes 1, Rennes,*
[7] *France.*
[8] [b]*Now at University of Liege, ArGEnCo, GEO[3], Hydrogeology and Environmental*
[9] *Geology, B52/3 Sart-Tilman, 4000 Liege, Belgium*

[10] **Abstract**

[11] The detection of preferential flow paths and the characterization of their
[12] hydraulic properties are major challenges in fractured rock hydrology. In this
[13] study, we propose to use temperature as a passive tracer to characterize frac-
[14] ture connectivity and hydraulic properties. In particular, we propose a new
[15] temperature tomography field method in which borehole temperature profiles
[16] are measured under different pumping conditions by changing successively
[17] the pumping and observation boreholes. To interpret these temperature-
[18] depth profiles, we propose a three step inversion-based framework. We con-
[19] sider first an inverse model that allows for automatic permeable fracture de-
[20] tection from borehole temperature profiles under pumping conditions. Then
[21] we apply a borehole-scale flow and temperature model to produce flowmeter
[22] profiles by inversion of temperature profiles. This second step uses inversion
[23] to characterise the relationship between temperature variations with depth
[24] and borehole flow velocities (*Klepikova et al.*, 2011). The third inverse step,

[*]Corresponding author
Email address: mklepikova@ulg.ac.be (Maria V. Klepikova)

₂₅ which exploits cross-borehole flowmeter tests, is aimed at inferring inter-

₂₆ borehole fracture connectivity and transmissivities. This multi-step inverse

₂₇ framework provides a means of including temperature profiles to image frac-

₂₈ ture hydraulic properties and connectivity. We test the proposed approach

₂₉ with field data obtained from the Ploemeur (N.W. France) fractured rock

₃₀ aquifer, where the full temperature tomography experiment was carried out

₃₁ between three 100 meter depth boreholes 10 meters apart. We identified sev-

₃₂ eral transmissive fractures and their connectivity which correspond to known

₃₃ fractures and corroborate well with independent information, including avail-

₃₄ able borehole flowmeter tests and geophysical data. Hence, although indirect,

₃₅ temperature tomography appears to be a promising approach for character-

₃₆ izing connectivity patterns and transmissivities of the main flow paths in

₃₇ fractured rock.

1. Introduction

₄₀ The accurate prediction of fluid flow in fractured media is a challenging

₄₁ problem, as flow may be localized in few small fractures with heterogeneities

₄₂ at all scales (e.g. *Berkowitz*, 2002). The classical approach to infer detailed

₄₃ flow properties relies on the identification of the flowing fractures followed

₄₄ by hydraulic testing with packers (e.g. *Shapiro and Hsieh*, 1998). Recent nu-

₄₅ merical developments (e.g. *Yeh and Liu*, 2000; *Brauchler et al.*, 2003; *Illman*

₄₆ *et al.*, 2009; *Berg and Illman*, 2013) have significantly improved hydraulic

₄₇ tomography methods in fractured media. However, spatial resolution of the

₄₈ inferred tomograms strongly depends on the number of observation intervals

2

49 (*Sharmeen et al.*, 2012). Furthermore, this approach requires the installation

50 of packers which is often not possible. To avoid these practical issues, we can

51 consider other types of data that can be more easily obtained and that are

52 directly sensitive to ground water flow.

53   Temperature data meet these conditions as geothermal heat can be con-

54 sidered as a natural tracer of groundwater flow (*Anderson*, 2005; *Saar*, 2011).

55 Furthermore, temperature profiles can be obtained easily and continuously in

56 space by logging a temperature probe in the observation borehole. The use

57 of fiber optic technology can also greatly improve the temporal and spatial

58 coverage of borehole temperature measurements (*Read et al.*, 2013). Temper-

59 ature data have often been used for inferring vertical or horizontal ground-

60 water flow velocities assuming homogeneous aquifer properties (*Bredehoeft*

61 *and Papadopulos*, 1965; *Reiter*, 2001; *Anderson*, 2005; *Saar*, 2011).

62   In fractured rocks, abrupt temperature changes are often observed at spe-

63 cific depths (e.g. *Ge*, 1998; *Bense et al.*, 2008; *Chatelier et al.*, 2011). When

64 groundwater flow occurs within a permeable fracture, it may perturb the

65 temperature profile within and around the fracture due to advected flow car-

66 rying either warmer or cooler fluid (*Ge*, 1998). In large-scale faults, velocities

67 can be large enough to influence the regional heat flux distribution (*Deming*,

68 1993; *Ge*, 1998; *Anderson*, 2005; *Saar*, 2011). Moreover, ambient flow in

69 boreholes themselves, that arises due to the difference in hydraulic heads be-

70 tween fractures intersecting the borehole, affects temperature borehole logs

71 (*Bidaux and Drogue*, 1993; *Pehme*, 2010; *Klepikova et al.*, 2011). A few

72 studies have considered borehole temperature profiles in fractured rocks un-

73 der induced fluid flow conditions (*Flynn*, 1985; *Silliman*, 1989). Among them

3

₇₄ *Silliman* (1989) argued that temperature anomalies produced by pumping in
₇₅ adjacent boreholes can be used for initial estimates of fractures connecting
₇₆ a given 'pumping-observation' borehole pair. Few of these studies, however,
₇₇ were able to quantify the fracture hydraulic properties or describe how these
₇₈ fractures form different flow paths. This is the objective of this study.

₇₉ Recently, we have shown how borehole temperature gradients may be
₈₀ sensitive to vertical borehole flow velocities (*Klepikova et al.*, 2011). By ap-
₈₁ plying a fluid flow and heat transfer forward numerical model, we were able
₈₂ to obtain borehole flow profiles under ambient, pumping (while pumping at
₈₃ the top of the borehole) and cross-borehole (while pumping in neighboring
₈₄ boreholes) flow conditions from borehole temperature-depth profiles. Fur-
₈₅ thermore, such flow profiles can be used to characterize the connectivity and
₈₆ hydraulic properties of the main flow paths in fractured rock (*Paillet*, 1998;
₈₇ *Le Borgne et al.*, 2006). The method is based on the idea that pumping mod-
₈₈ ifies hydraulic heads in flow paths intersecting a pumping borehole, which in
₈₉ turn produce changes in vertical borehole flow in observation boreholes. In a
₉₀ recent study, a new inversion method was developed to invert such borehole
₉₁ flow data. This approach, referred as flow tomography (*Klepikova et al.*,
₉₂ 2013), was successful in estimating inter borehole fracture hydraulic proper-
₉₃ ties as well as fracture connectivity on synthetic examples. Here, we propose
₉₄ to investigate how both approaches may be coupled to invert borehole tem-
₉₅ perature data in different flow conditions to estimate fracture connectivity
₉₆ and hydraulic properties between pairs of boreholes.

₉₇ In this contribution, we propose a multi-stage inversion framework to in-
₉₈ terpret temperature measurements obtained during sequential cross-borehole

4

99 pumping tests. We propose to call such experiments as passive temperature

100 tomography experiments. The term "passive" means that temperature is

101 used as a passive tracer without any heat injection, in contrast to the ap-

102 proach taken in other recent works (*Leaf et al.*, 2012; *Read et al.*, 2013;

103 *Wagner et al.*, 2013). Although this study makes use of the methodolo-

104 gies presented in (*Klepikova et al.*, 2011) and (*Klepikova et al.*, 2013), it

105 presents three novelties with respect to these previous works. First, in the

106 present study we propose a new method for automatic inversion of borehole

107 temperature profiles that significantly facilitate data interpretation. The to-

108 mography approach based of borehole temperature measurements presented

109 here is analogous to the flow tomography approach (*Klepikova et al.*, 2013).

110 However, an important advantage of this new method over direct flow mea-

111 surements is that temperature can be measured more easily and continuously.

112 Finally, this study presents the first application of this method using a to-

113 mographic approach in a fractured rock site.

114   In the first part we briefly review the source of temperature variations

115 in the subsurface and examine under which conditions and assumptions our

116 inverse approach may be applied. We then present the methods used in the

117 inversion procedure. In the third part, we describe the experimental site

118 and the temperature tomography experiment conducted. Finally, we present

119 and discuss the results of the application of the inverse approach to three

120 boreholes from the experimental field site.

5

2. Background and Methodology Proposed

In the near surface, temperature-depth profiles are influenced by seasonal temperature variations of the land surface. Typically, this zone includes the first ten meters below the ground, although this depends on the local thermal properties. Below this depth, the temperature gradient is influenced by the heat flux, the thermal conductivity of rocks (*Freifeld et al.*, 2008), radioactive heat sources (*Perry et al.*, 2006) and longer term climate variations (e.g. *Ferguson*, 2006). Moreover, depending on hydrogeological parameters, groundwater flow may have a significant effect on the subsurface temperature regime (e.g. *Anderson*, 2005; *Ferguson*, 2006). To characterize the factors that control heat transfer in the subsurface, precise measurements of temperature as a function of depth should be considered.

In this study we focus on permeable fractured rocks in the upper crust (typically above 200 meters deep), where advection can have a significant effect on the subsurface temperature. We assume that the temperature gradient in the regional rock mass increases monotonically (i.e. constant geothermal gradient) (*Klepikova et al.*, 2011). Given typically small temperature ranges for this depth, the dependence of viscosity on temperature is neglected. In such media induced or natural localized fracture flow generally creates local temperature anomalies. An example of flow and temperature pattern for two boreholes connected by one main flow path under ambient, single and cross-borehole pumping conditions is shown in Figure 1. In such a system, heat is carried by vertical borehole flow and dissipates to the surrounding rocks. Hence, borehole flow under ambient (Figure 1A) and pumping conditions (Figure 1B) significantly disturb the equilibrium bore-

6

146 hole temperature profiles.

147   Ambient vertical borehole flow is induced by differences in hydraulic head
148 between the different flow paths that intersect observation boreholes (e.g.
149 *Pehme*, 2010; *Klepikova et al.*, 2011). These differences in hydraulic heads
150 are in general due to regional flow conditions (e.g. *Elci et al.*, 2001) and the
151 resulting vertical borehole flow may significantly disturb the temperature
152 profile (e.g. *Chatelier et al.*, 2011) (well 1, Figure 1A). When pumping in one
153 of the wells, hydraulic head changes occur in the flow path connected to the
154 pumping well. The flow paths connecting a borehole pair transmit hydraulic
155 head variations to the neighbor borehole. This difference in hydraulic heads,
156 in turn, depends on the transmissivities of the connecting fractures. For
157 instance, in Figure 1B the upflow in the observation well 1 is maximum since
158 only the upper fracture is connected and transmits the drawdown induced
159 by pumping, implying a temperature increase in the well 1 in response to
160 pumping from the well 2. In the well 2 (Figure 1B), an increase of the flow
161 velocity above flowing fractures in the pumping borehole implies that the
162 water flowing in the borehole has less time to exchange heat with surrounding
163 rocks hence it also implies temperature profile perturbations.

164   Here we propose a multi-stage tomography approach based on an inverse
165 framework for the interpretation of temperature profiles under combinations
166 of pumping conditions to infer the full connectivity pattern as well as fracture
167 hydraulic properties. The inversion framework proposed in this study has
168 three main steps :

169   1. Automatic detection of fracture zones intersecting each borehole by
170   applying changepoint modelling to temperature profiles under ambient

7

[171] flow conditions and steady pumping flow conditions.

[172] 2. Coupled fluid flow-heat transfer modelling: inversion of temperature
[173] profiles under ambient, single and cross-borehole flow conditions to
[174] derive flow profiles.

[175] 3. Estimation of fracture hydraulic properties and connectivity between
[176] and around each borehole pair by applying flow tomography to ambient,
[177] single and cross-borehole pumping flowmeter profiles obtained from the
[178] previous step.

[179] The approach is summarized in Figure 2. In the following sections we
[180] detail the main steps.

[181] *2.1. Permeable Fracture Identification at Borehole Scale*

[182] The first step in inferring the flow pattern between a borehole pair is the
[183] detailed characterization of flow properties at the borehole scale. Several
[184] methods may be used for identification of permeable/transmissive fractures
[185] at the borehole scale. These include, for example, geological/geophysical
[186] methods (*Genter et al.*, 1997), such as the inspection of continuous core,
[187] caliper data, acoustic and optical televiewing (*Barton and Zoback*, 1992)
[188] and electrical resistivity measurements (*Keys*, 1979). Other methods include
[189] hydraulic testing, such as flowmeter tests (*Paillet*, 1998), including heat-pulse
[190] flowmeter(e.g. *Le Borgne et al.*, 2007), impeller tests (e.g. *Newhouse*, 2005),
[191] high spatial resolution temperature profiling (*Mwenifumbo*, 1993; *Barton et
[192] al.*, 1995) and flexible liner profiling (*Pehme*, 2010, 2013).

[193] In this study, we propose an automatic permeable fracture identification
[194] method based on borehole temperature profiles, that takes the advantage

8

of the close relationship between the borehole temperature gradient and the vertical borehole flow velocity (*Pehme*, 2010; *Klepikova et al.*, 2011). An illustration of temperature profiles under ambient and pumping flow conditions is given in Figure 1. In this example, abrupt changes in temperature gradient occur at depths where transmissive fractures intersect the borehole. As borehole flow in fractured aquifers is characterized by intervals of constant flow between transmissive fractures (*Paillet*, 1998), inflow points for each borehole can be therefore identified by inspection of temperature profiles.

In the field, however, multiple sources of error such as uncertainty about rock thermal diffusivity, changes in borehole diameter, multiple fracture zones and temperature measurement errors, may influence temperature data (*Klepikova et al.*, 2011). The noise in the temperature measurements related to these factors complicates the identification of changes in temperature gradient trends and the detection of flowing fractures. To interpret the temperature-depth profiles objectively, we apply a recently proposed changepoint model (*Gallagher et al.*, 2011). Changepoints can be defined as abrupt changes in trends (such as the mean, gradient or any function) over depth or time. Between changepoints it is assumed that underlying trends in the data are either constant or vary linearly with depth. The goal is to infer the location of changepoints (as well as the noise variance associated with each dataset if desired) in a noisy data series without a priori knowledge of the number of changepoints. Ideally, then, changepoint modelling allows us to identify inflow and outflow zones from temperature profiles.

The approach uses transdimensional Markov chain Monte Carlo to sam-

9

₂₂₀ ple many possible solutions with different numbers and locations of change-
₂₂₁ points and noise estimates which are either accepted or rejected, based on
₂₂₂ probabilistic criterion (*Gallagher et al.*, 2011). In general, identification of
₂₂₃ the location and number of changepoints is directly influenced by the noise
₂₂₄ level in the data and the variability of the observations about the mean be-
₂₂₅ tween changepoints is indicative of the level of noise. Thus, data with lower
₂₂₆ noise tend to produce a model with many changepoints, while models with
₂₂₇ fewer changepoints will be acceptable for data with higher noise. The ap-
₂₂₈ proach is formulated in a Bayesian framework, which naturally balances the
₂₂₉ noise level with the complexity of the changepoint structure (*Gallagher et al.*,
₂₃₀ 2011). Therefore, given a choice between simple and complex models that
₂₃₁ provide a similarly adequate fit to the observed data, the models with fewer
₂₃₂ changepoints will be favored. We demonstrate that application of change-
₂₃₃ point model to temperature profiles allows for automatic fracture detection
₂₃₄ in a field example. Note, that this result can have also a practical implica-
₂₃₅ tion for hydrocarbon recovery, where temperature logs are commonly used
₂₃₆ to estimate fluid inflow during hydrocarbon production (e.g. *Williams et al.*,
₂₃₇ 2000).

₂₃₈ *2.2. Inverse Modeling of Borehole Temperature Profiles for Flow Estimation*

₂₃₉   The second step is the inversion of borehole temperature profiles to flow
₂₄₀ profiles. For a borehole with no flow, the downhole temperatures are assumed
₂₄₁ to follow the geothermal gradient while a reduced temperature gradient im-
₂₄₂ plies an increase of the flow velocity under single or cross-borehole flow con-
₂₄₃ ditions (*Klepikova et al.*, 2011). In order to study flow and heat transfer at
₂₄₄ the borehole scale, we use a numerical model described in detail in *Klepikova*

10

245 *et al.* (2011).

This model considers a cylindrical borehole (with a radius fixed to r_0) surrounded by the rock matrix. The borehole is divided into sections according to the position of flowing fractures inferred from the changepoint modeling (Figure 3). Note, that we do not model the fracture outside the borehole. The model includes heat advection in the borehole with a constant vertical laminar flow and heat dissipation in the surrounding rock matrix. The heat transfer equation under steady state conditions is given by

$$\nabla \cdot (\alpha_i \nabla \theta) - v \nabla \theta = 0, \tag{1}$$

where θ is temperature, v is the borehole flow velocity, $i = \{Fluid, Rock\}$, $\alpha_i = k_i / \rho_i C_i$ is the thermal diffusivity, k_i is the thermal conductivity, C_i is the heat capacity, and ρ_i is the density. At the bottom of each borehole section we impose the borehole flow as the sum of all fractures inflows and outflows below the modeled section (Q_{fr}). The inflow temperatures (here the bottom temperature for each section) are taken from the measured temperature profile. The rock temperature at the outer vertical boundary is taken from the temperature profile measured in the borehole not affected by vertical flow (the ambient temperature in the rock). The boundary condition at the lower boundary is taken as a background geothermal heat flux (Figure 3).

$$Q = -k_{rock} \gamma, \tag{2}$$

246 where γ is the background geothermal gradient. The temperature at the up-
247 per boundary is taken as the surface temperature (or from other constraints
248 such as the temperature of a sub-horizontal large-scale fracture).

11

In this study we propose a new method for automatic inversion of borehole temperature profiles, that significantly facilitates data interpretation. In order to invert temperature profiles to infer flow profiles, we couple the forward model of heat and fluid flow at the borehole scale (*Klepikova et al.*, 2011) with an optimization algorithm. The inverse problem consists of estimating the vertical borehole flow velocities that perturb the temperature profiles observed under different flow conditions. The misfit function, FO, which evaluates the difference between direct model simulations and temperature measurements, is given by

$$FO = \frac{1}{\sigma_\theta^2} \frac{1}{N_\theta} \sum_1^{N_\theta} (\theta_{obs} - \theta_{mod})^2 \qquad (3)$$

where θ_{obs} are the observed temperatures, θ_{mod} are the temperatures predicted by the model, σ_θ is the noise variance associated with temperature data and N_θ are the number of temperature observations. As we show later, the typical objective function for this problem is convex and has a global minima. The optimization problem is solved by the Nelder-Mead Simplex (NMS) algorithm incorporated in the MATLAB optimization Toolbox (*Lagarias et al.*, 2011). The NMS algorithm is a nonlinear fast local search method that does not require derivatives of the objective function and is suited to our problem.

The uncertainty in the flow velocity values obtained from temperature profiles depends on the length of the borehole flowing sections, the temperature tool precision, and the flow velocity (*Klepikova et al.*, 2011). In order to consider the whole range of possible flow velocities for which the difference between the simulated and measured temperature is less than the relative

12

₂₆₃ accuracy of the probe, the objective function was normalized to the data er-

₂₆₄ ror (Equation 6). Thus the magnitude of the data errors influence the value

₂₆₅ of the objective function and the convergence criteria is reached when the

₂₆₆ objective function value equals one. Then, when we fit the data, on average,

₂₆₇ to within the error, all the solutions for which the objective function value is

₂₆₈ in the order of one are acceptable.

₂₆₉ *2.3. Site Scale Flow Inverse Modeling*

₂₇₀ Once the borehole flow profiles have been inferred from the tempera-

₂₇₁ ture profiles, these can be used in order to estimate transmissivities of hy-

₂₇₂ draulically active fractures between and around the pumping and observation

₂₇₃ boreholes (*Paillet*, 1998; *Le Borgne et al.*, 2007; *Paillet et al.*, 2012). At the

₂₇₄ borehole scale, pumping induces flow in the different fractures intersecting

₂₇₅ the pumping borehole (Figure 1B). The resulting vertical flow depends on

₂₇₆ fracture transmissivities locally to the borehole. At larger scale, pumping

₂₇₇ induces hydraulic head variations in flow paths, which in turn drives vertical

₂₇₈ flow variations between the fractures intersecting the observation borehole.

₂₇₉ The induced vertical flow in the observation borehole depends on the differ-

₂₈₀ ent transmissivities of connecting fractures. In particular, the magnitude and

₂₈₁ the direction of the vertical flow velocity depends on the difference between

₂₈₂ transmissivities of fractures that connect the borehole as well as transmis-

₂₈₃ sivities of fractures that interconnect fractures connected to the borehole

₂₈₄ (*Klepikova et al.*, 2013).

₂₈₅ Fracture networks often have several sets of fracture connections and in-

₂₈₆ terpretations of the results are not straightforward. Recently, we have pro-

₂₈₇ posed an inverse modelling framework for flow tomography data that invert

13

₂₈₈ single- and cross-borehole flow profiles in order to estimate transmissivities of

₂₈₉ hydraulically active fractures between and around the pumping and observa-

₂₉₀ tion boreholes (*Klepikova et al.*, 2013). This inverse modelling approach uses

₂₉₁ a 3-D steady state numerical flow model (with 2-D flow in each fracture) to

₂₉₂ reproduce borehole flow profiles and borehole drawdowns in a fracture net-

₂₉₃ work. We assume a Darcy flow in the fractures, and the volume flow rate

₂₉₄ per unit fracture length on the fracture is given by

$$u = -\frac{k}{\mu}d\nabla p, \tag{4}$$

where k describes the fracture permeability (m^2), d is the fracture aperture (m). Each fracture is characterized by a value of transmissivity T, which is given by

$$T = d\frac{k\rho g}{\mu}. \tag{5}$$

We apply zero-head boundary conditions, that means that no ambient flow takes place in the boreholes. Hence, the model results can be compared to field data, with the ambient flow profile substracted from the pumping profiles (*Paillet*, 1998). In the following flow models, the fracture aperture is fixed at $d = 1 \cdot 10^{-3}$ m, which is a realistic value as deduced from tracer tests conducted on the same site. To estimate the fracture transmissivities from the cross-borehole flow profiles inferred from the temperature profiles and drawdown measurements we coupled the direct flow model with a quasi-Newton optimization algorithm. The misfit function, FO, which evaluates the difference between flow model simulations and observations, is given by

$$FO = \frac{1}{\sigma_s{}^2}\frac{1}{N_s}\sum_0^{N_s}\left(s_{obs} - s_{mod}\right)^2 + \frac{1}{\sigma_v{}^2}\frac{1}{N_v}\sum_0^{N_v}\left(v_{obs} - v_{mod}\right)^2, \tag{6}$$

14

295 where v_{obs} and s_{obs} are the flowmeter and drawdown observations, σ_v and

296 σ_s are data errors for flow and drawdown respectively, N_v and N_s are the

297 numbers of observations for flow and drawdown respectively, v_{mod} and s_{mod}

298 are the velocity and drawdown predicted by the model.

299 We use a simplified fracture network model that attempts to reproduce

300 basic fracture network connectivity without representing explicitly the com-

301 plete fracture geometry (length, orientation, dip). Solving the fracture net-

302 work geometry is not expected to be possible without additional geophysical

303 data and so we refer to the effective or apparent connectivity to highlight the

304 simplification. In the fracture network model, the observation and pumping

305 boreholes are both intersected by horizontal fractures that represent frac-

306 tures identified previously at borehole-scale (Section 2.1). The horizontal

307 fractures are connected by a vertical fracture equidistant from both bore-

308 holes, which allows to take into account cross connections between fractures.

309 The apparent or effective connectivity between boreholes is simply controlled

310 by attributing different values of transmissivity to the different sections of

311 the vertical fracture.

312 An example of the simplified fracture network is given in Figure 2d. We

313 first define local transmissivities of each fracture zone intersecting the ob-

314 servation and pumping boreholes ($T_{B1-1,2}$ and $T_{B2-1,2}$ in Figure 2d) through

315 the inversion of ambient and steady pumping single-borehole flow profiles.

316 In this case the number of parameters ($T_{B1-1,2}$ and $T_{B2-1,2}$) equals to the

317 number of observations (1 drawdown and 1 vertical borehole flow velocity

318 for each well). Then, the inverse approach adjusts transmissivities of the

319 different sections of the vertical fracture (T_1, T_2 and T_3 in Figure 2d), so

15

320 that the simulated cross-borehole profile and drawdown in observation well
321 matches the data. In order to reduce the uncertainty in the model calibra-
322 tion, we perform a joint inversion of two pumping tests where the pumping
323 and observation boreholes are reversed for each pair of boreholes. We thus
324 use 4 observations (s_1, s_2, v_1 and v_2) in order to determine 3 parameters.
325 Furthermore, we believe that more complex fracture connection patterns in
326 the interval between the boreholes could be approximated by combination
327 of basic kinds of connections and we introduce an order of complexity that
328 matches the information content of the data. These steps allow the inference
329 of the apparent connectivity and transmissivities of the main flow paths as
330 well as the transmissivity of fractures that connect the flow paths but do not
331 cross the boreholes.

332 3. Experimental Setting

333 3.1. Experimental Site

334 The temperature tomography experiments were carried out within a frac-
335 tured rock aquifer at the test-site Stang er Brune (Ploemeur, France) (*Le*
336 *Borgne et al.*, 2007). The site consists of 4 boreholes: borehole B1 (83 m
337 deep), boreholes B2 and B3 (100 m deep) and borehole F22 (70 m deep). B1,
338 B2 and B3 form a triangle within a radius of 10 m and F22 is 30 m from this
339 triangle (Figure 4A). The geology of the site is characterized by a gently dip-
340 ping contact between granite and overlying micaschists. This contact zone
341 intersects boreholes at the following depths: B1 at 38 m, B2 at 37 m, B3 at
342 37.5 m, and F22 at 13 m. Both hydrological and borehole data (*Le Borgne et*
343 *al.*, 2007) demonstrate the presence of a shallow fracture within a mica-schist

16

³⁴⁴ formation dipping parallel to the contact zone between granite and overlying
³⁴⁵ micaschists and intersecting all the boreholes at the site. Moreover, B1, B2
³⁴⁶ and B3 boreholes are intersected by several permeable fractures within the
³⁴⁷ granite formation (*Le Borgne et al.*, 2007; *Dorn et al.*, 2012, 2013). The
³⁴⁸ site is located near a lake and there is a regional or watershed scale upward
³⁴⁹ flow at this location, resulting from hydraulic head difference between the
³⁵⁰ deepest confined fractures in granite and the upper mica schist. Flow mea-
³⁵¹ surements demonstrated that F22 borehole is not affected by vertical flow.
³⁵² In the next section, we demonstrate that temperature measurements on the
³⁵³ site are strongly influenced by these hydrogeological conditions.

³⁵⁴ *3.2. Borehole Temperature Profiles in Ambient Conditions*

³⁵⁵ Temperature measurements were conducted under ambient flow condi-
³⁵⁶ tions with a temperature logging device, the Idronaut CDT 302 Multi-Parameter
³⁵⁷ Probe with a tool precision of $0.005°C$ (Figure 4C). All four wells show abrupt
³⁵⁸ changes in temperature gradient between 10 and 40 meters depth, the exact
³⁵⁹ depth depending on the borehole. Below this depth, the temperature gradi-
³⁶⁰ ent is relatively low and variable between the different boreholes. Above this
³⁶¹ depth, the temperature gradient changes to conform to the surface tempera-
³⁶² ture, which is fixed by the mean annual surface temperature equal to about
³⁶³ $T_{surf} = 12.5°C$.

³⁶⁴ The observed site-scale temperature field is typical of the one perturbed
³⁶⁵ by a gently dipping structure where fluids of greater temperature than the
³⁶⁶ surrounding rocks are flowing from depth to sub-surface (e.g. *Ge*, 1998; *Saar*,
³⁶⁷ 2011). The corresponding flow pattern is shown in Figure 4B. For each
³⁶⁸ borehole, the depths of change in gradient, F22 at 8 *m*, B1 at 24 *m*, B2 at 25

17

369 m and B3 at 36.5 m, correspond to the depths of the first shallow fracture
370 in mica-schists, which was reported by *Le Borgne et al.* (2007). Fluid flow in
371 this fracture advects heat and because water in the conduit is assumed well
372 mixed it provides a constant temperature boundary condition. Consequently,
373 this process distorts the otherwise continuous linear geothermal profile (*Saar*,
374 2011).

375   Below the sub-horizontal fracture in mica-schist, the boreholes have dif-
376 ferent temperature gradients. The highest thermal gradient $\gamma = 0.016\ ^\circ C/m$
377 was measured in the F22 well. This borehole has no significant ambient verti-
378 cal flow due to its very low permeability and so the temperature field is dom-
379 inated by the upward conductive heat transfer. Thus, the F22 temperature-
380 depth profile may be considered representative of the temperature of the
381 surrounding rock at the site.

382   While this groundwater flow in the mica-schist influences the tempera-
383 ture field of the whole site, the temperature gradients variations in granite
384 seem to have much less regional influence. In boreholes B1, B2, and B3 the
385 temperature gradients measured below 30-40 meters are typically lower than
386 the geothermal gradient estimated from F22. This is the result of upward
387 advective flow between flowing fractures as revealed by borehole flow logs
388 (*Klepikova et al.*, 2011).

389   Furthermore, for all boreholes a slight change in temperature gradient is
390 observed at the depth of the contact zone between granite and micaschists
391 (see previous section), that is shown by the black line in Figure 4C. These
392 thermal gradient variations are due to the higher thermal conductivity of
393 granite compared to micaschists. Moreover, the B3 temperature profile in

18

394 Figure 4 shows abrupt temperature changes at 45 m and 80 m, which cor-
395 respond to depths of fractures reported by *Le Borgne et al.* (2007). These
396 anomalies are explained by the localized lateral advection of colder water
397 within narrow fractures in granite intersecting the borehole (*Ge*, 1998). To
398 summarize our observations, the borehole temperature distributions reflect
399 five dominant factors:

400 • upward conductive heat transfer through the rocks reflected as a con-
401   tinuous increase of temperature with depth,

402 • gently dipping groundwater flow in micaschists of warmer (deeper) ori-
403   gin,

404 • advection of heat by the vertical flow in the boreholes,

405 • localized lateral advective transfer of water within narrow fractures,

406 • variations in thermal properties of rock.

407 *3.3. Temperature Tomography Experiments*

408 After measuring the ambient temperature profiles and hydraulic heads
409 in all boreholes, three successive cross-hole pumping tests were conducted
410 in B1, B2 and B3 with temperature monitoring in all boreholes. For the
411 temperature tomography study, the temperature profiles need to be measured
412 a sufficient time after pumping to ensure steady state has been reached. To
413 monitor this, a set of 7 thermistors was centered permanently within each
414 well. The number of transducers was chosen to be able to control all borehole
415 sections between the flowing fractures. To record temperature variations

19

416 with time for the given depths, the acquisition time of 20 s was chosen.
417 An example of temporal evolution of temperature is given in Figure 5D.
418 These data show that thermal steady state for each particular depth and
419 well was reached in $1-2$ hours after switching on the pumping, depending
420 on the pumping and observation locations. The temperature variations with
421 time were not used in the subsequent analysis for this study. However, the
422 interpretation of transient data could also provide other useful information,
423 such as thermal diffusivity values.

424 Prior to starting the next pumping test the pressure and temperature
425 were allowed to recover for each experiment. The first cross-borehole pump-
426 ing test took place in well B3 with a pumping rate of $Q_{B3} = 154 \pm 3$
427 l/min. Subsequently, we conducted pumping tests in B2 well (pumping rate
428 $Q_{B2} = 136 \pm 14\ l/min$), and then in B1 well (pumping rate $Q_{B1} = 77 \pm 2$
429 l/min). Thus, the full data set consists of 9 hydraulic heads and 9 tem-
430 perature profiles: 3 ambient profiles and 6 profiles when pumping in the
431 neighboring well. The temperature profiles were measured with a tempera-
432 ture logging device (The Idronaut CDT 302 Multi-Parameter Probe). During
433 the experiment it was observed that upward temperature logs often exhibit
434 slightly higher temperatures than downward logs. In this work we consid-
435 ered only downward logs, as we believe that it creates less perturbation of
436 the temperature field. The collected steady-state temperature-depth profile
437 are shown in Figure 5, and these clearly show the sensitivity of temperature
438 measurements to changes in pumping conditions.

20

4. Results

In this section, we present results of the application of the inverse modelling framework to data from Stang er Brune field site. We firstly infer the location and number of flowing fractures intersecting the boreholes by applying changepoint modelling to temperature profiles. Then, we assess inter-borehole connections properties by inverting the temperature tomography data set. Finally, we discuss the corresponding uncertainty estimates.

4.1. Permeable Fracture Identification at Borehole Scale

In order to detect flowing fractures intersecting the boreholes, we apply changepoint modelling e.g. (*Gallagher et al.*, 2011) to temperature profiles under ambient and single-borehole pumping flow conditions. Figure 6 presents ambient (A) and pumping (B) temperature profiles (with a pumping rate $Q = 20\ l/min$) measured in B1 borehole, the inferred changepoint structures (red line) and probability distributions on the changepoint locations for both flow conditions. These change point structures were determined assuming that the noise level for these temperature data equal to the $\pm 0.005\ ^{\circ}C$, that correspond to the precision of the tool. Locations of the changepoints inferred from the temperature profile under ambient flow conditions are the following: $z = 24$ and $38\ m$. They correspond to the depths of the first shallow fracture in mica-schists and the depth of the contact zone between granite and mica-schists. As discussed in the section 3.2, the contrast in gradient at the depth of the first shallow fracture in mica-schists is due to constant temperature boundary condition, provided by this fracture. The change in gradient at $38\ m$ in B1 is due to the contrast in thermal conductivity of the

21

$_{463}$ surrounding rocks. This example demonstrates that analysis of temperature

$_{464}$ profiles under ambient conditions can reveal changes in temperature gradient

$_{465}$ that are not related to flow in the borehole itself (e.g. contrast in thermal

$_{466}$ properties of rock, low transmissive fractures carrying flow of contrast tem-

$_{467}$ perature).

$_{468}$ The locations of the most probable changepoints inferred from the tem-

$_{469}$ perature profile under pumping conditions are the following: $z = 24, 50.9$,

$_{470}$ 60.9 and 78.7 m. They correspond well to fracture locations in B1, identified

$_{471}$ previously by flowmeter tests (*Le Borgne et al.*, 2007) and ground-penetrating

$_{472}$ radar (*Dorn et al.*, 2012). The increase in the number of inferred change-

$_{473}$ points for the pumping conditions means that the sensitivity of the method

$_{474}$ could be improved by increasing the pumping rate. However, as discussed in

$_{475}$ *Klepikova et al.* (2011) there is a limited range of flow velocities for which

$_{476}$ changes in flow produces measurable changes in the thermal gradient. Thus,

$_{477}$ for too large flow velocities the temperature anomaly propagates too fast to

$_{478}$ allow for measurable loss of heat to the rock formation. For too small flow

$_{479}$ velocities, the temperature anomaly equilibrates quickly with the surround-

$_{480}$ ing rock temperature. In practice, the estimated temperature changes in a

$_{481}$ given borehole section between two flowing fractures should be larger than

$_{482}$ the measurement error. For our experimental conditions, we found that the

$_{483}$ value of $Q = 20 \ l/min$ is optimal as further increasing the pumping rate

$_{484}$ implies that the temperature profile would appear to be completely straight.

$_{485}$ After applying the changepoint modelling method to other boreholes, the

$_{486}$ depths of the inferred most probable changepoints are $z = 24, 56$ and 79

$_{487}$ in B2 borehole and $z = 35, 45$ and 80 in B3 borehole. These depths are

22

488 also consistent with fractures that were identified as being transmissive by

489 single-borehole flowmeter tests (*Le Borgne et al.*, 2007), demonstrating the

490 potential of changepoint modelling in the automatic detection of the main

491 transmissive fractures from temperature profiles.

492 *4.2. Inverse Modeling of Borehole Temperature Profiles for Flow Estimation*

493 Having detected the flowing fractures, we simulate flow and temperature

494 advection for each borehole from the first bottom transmissive fracture up

495 to the shallowest transmissive fracture. The rock temperature at the outer

496 boundary of the model borehole is inferred from the temperature profile mea-

497 sured in F22 as it is not affected by borehole flow. The thermal properties

498 of the rock matrix were chosen to be equal to the mean thermal properties

499 measured in laboratory on samples from B1 borehole. Note, that we tested

500 in our numerical model what could be the consequence of uncertainties about

501 thermal conductivity and we found that the resulting uncertainty about ve-

502 locity estimation remains within a few percent. Thus, the granite thermal

503 conductivity is given by $k_{Rock} = 3.31 \ W/m°C$, the heat capacity of the gran-

504 ite is given by $C_{Rock} = 738 \ J/kg°C$. The values for water properties are given

505 by $k_{Fluid} = 0.59 \ W/m°C$ and $C_{Fluid} = 4189 \ J/kg°C$ respectively (*Incropera*

506 *and DeWitt*, 1996).

507 A typical example of the objective function versus the vertical borehole

508 flow velocity is presented in Figure 7. In this figure the optimal flow velocity

509 (v_{opt}) is presented for the part of temperature profile measured in B1 borehole

510 (over the depth range $60.9 − 78.7 \ m$) while pumping in B2. In order to quan-

511 tify the uncertainty on this flow velocity, we determine the range of possible

512 flow velocities (v_{min}, v_{max}) for which the objective function is less than one

23

513 and thus the difference between the simulated and measured temperature is

514 less than the relative accuracy of the probe (Equation 6). The objective func-

515 tion is found to be most sensitive for $v = 5 \cdot 10^{-4} - 2 \cdot 10^{-3} \ m/s$ flow velocity

516 range. For larger velocities the temperature anomaly propagates too fast to

517 allow for significant temperature change by heat loss to the rock formation.

518 Then for flow velocities larger than $v = 2 \cdot 10^{-2} \ m/s$ the temperature profile

519 becomes completely straight and the objective function becomes insensitive

520 to velocity. It is difficult to affirm that we found a global minima. However,

521 for all cases considered in this study, the objective function was found to be

522 smooth and convex thus enable efficient minimization.

523   The inversion results show that vertical borehole flow occurs in all bore-

524 holes under ambient conditions. In order to check the accuracy of the es-

525 timated flow profiles, we measured flow profiles directly with heat-pulse

526 flowmeter for some hydrodynamic conditions (ambient and during pump-

527 ing in B2 borehole). The heat pulse flowmeter can measure flow velocities as

528 small as 0.5 L/min (*Paillet*, 2004). The uncertainty on the velocity values

529 obtained from temperature profiles varies between 0.1 and 0.5 L/min de-

530 pending on the length of the borehole flowing sections and the flow velocity.

531 The flow velocities obtained from temperature measurements are compared

532 in Figure 8 to flow measured directly with a flowmeter under the same hy-

533 drodynamic conditions. It appears that the method allows the reliable esti-

534 mation of flow velocities for a large range of flow, although the model slightly

535 underestimates flow for larger flow velocities. A possible reason for this may

536 be that the upper limit of the applicability of the model was reached for this

537 particular borehole section. Overall, however, the inversion of all measured

24

₅₃₈ temperature profiles provides a complete and continuous flow velocity data
₅₃₉ set for flow tomography.

4.3. Site Scale Flow Inverse Modelling

₅₄₁ We now apply the flow tomography framework in order to estimate the
₅₄₂ transmissivities of hydraulically active fractures between and around each
₅₄₃ borehole pair. To model flow between boreholes, the fracture network geom-
₅₄₄ etry has been simplified as described in Section 2.3 and we couple the forward
₅₄₅ model with the inverse algorithm. The partial differential equation (Equa-
₅₄₆ tion 4) was solved with the finite element code Comsol Multiphysics 4.2a
₅₄₇ with a fine tetrahedral meshing. A set of 20 starting transmissivity models
₅₄₈ is generated for each boreholes pair to search for a minimum of the objective
₅₄₉ functions. Note that the computation time for one direct simulation is about
₅₅₀ 2 minutes, while the solution converges generally after several hundred iter-
₅₅₁ ations. Thus, the number of starting points was limited by computing time
₅₅₂ for these modelling runs. For each borehole pair several solutions were found
₅₅₃ to satisfy the convergence criteria. As all acceptable solutions were found
₅₅₄ to be similar (except few cases discussed below), we consider only the 'best'
₅₅₅ solution providing the minimum of the objective function. Nevertheless, we
₅₅₆ accept the possibility that some solutions may correspond to local minima of
₅₅₇ the objective function. This can be addressed to some extent by increasing
₅₅₈ the number of the starting models if desired.

₅₅₉ The inverted parameter estimates are shown in Figures 9, 10 and 11 and
₅₆₀ synthesized in Table 1. Our results show that fracture transmissivities at the
₅₆₁ site range from 10^{-6} to $2 \cdot 10^{-3} \ m^2/s$, which is in general agreement with other
₅₆₂ studies at the same site (*Le Borgne et al.*, 2007; *Dorn et al.*, 2012, 2013). The

25

563 obtained solution yields the best fit to measured borehole drawdowns and the
564 flow tomography data inverted from temperature profiles. The comparison
565 of flow tomography data, including drawdowns s and variations of vertical
566 borehole flow velocities during cross-borehole pumping Δv in observation
567 boreholes, and inversion results is given in Table 2. This shows that the
568 predicted and measured flow and drawdowns values are generally in good
569 agreement for the cross-borehole tests.

570 To explain qualitatively the results, we discuss the relationship between
571 the inferred connectivity patterns (transmissivities of different sections of the
572 vertical fracture T_i) and variations of vertical borehole flow velocities during
573 cross-borehole pumping. The results for the B1-B2 borehole pair (Figure 9,
574 Table 1) demonstrate that the most transmissive fracture connection is the
575 one at a depth of 50 m that connect B1-3 and B2-2 fractures ($\log T_3 = -2.8$).
576 In contrast, the deep fractures, B1-4 and B2-4, are found to be poorly con-
577 nected ($\log T_5 = -5.8$). These results can be understood with reference to
578 Table 2, where flow tomography data (drawdowns s and variations of vertical
579 borehole flow velocities Δv during cross-borehole pumping tests in observa-
580 tion boreholes) are presented. For the B1-B2 borehole pair, we found an
581 increase of upward flow for all sections of both boreholes. Flow in the ob-
582 servation well is directly towards the fracture that transmits most drawdown
583 from the pumping well. Thus, this explains the strong connection found
584 for B1-3 and B2-2 fractures and it implies that overall transmissivities of
585 fractures connecting the B1-B2 borehole pair should decrease with depth.
586 Similarly, for the B1-B3 and B2-B3 borehole pairs, an increase in upward
587 flow in both boreholes during cross-borehole pumping tests (Table 2) implies

26

588 good fracture connections for the shallow fracture and less connectivity of
589 deep fractures.

590 For the fracture connection discussed above, the transmissivities T_i were
591 similar for all solution. However, for few cases the parameter estimations
592 were found to be uncertain. In order to explain this we refer to the sensi-
593 tivity analysis for flow tomography approach conducted in our recent study
594 (*Klepikova et al.*, 2013). This sensitivity analysis demonstrates that for small
595 borehole flows, similar velocities can be produced by different combinations
596 of fracture transmissivities, implying that the uncertainty about parameter
597 estimations increases as borehole flow decreases. Thus, large flow velocities
598 in deep borehole sections (Table 2) provide a strong constraint for deep frac-
599 ture connections for the B1-B2 and B1-B3 borehole pairs. For instance, for
600 the B1-B2 borehole pair, to maximize the difference in hydraulic heads draw-
601 ing these velocities, the transmissivity of the T_3 fracture connection should
602 be maximized, while the transmissivity of the T_4 fracture connection should
603 be minimized. In contrast, small flow velocities in shallow borehole sections
604 implies that the estimates of the parameters T_1 and T_2 are rather uncertain.
605 For the fracture network connecting the B2-B3 borehole pair, small flow ve-
606 locities in both wells (Table 2), do not provide a strong constraint for the
607 interconnection fracture transmissivities and the estimations of T_2, T_3 and
608 T_4 vary within two orders of magnitude.

609 The most transmissive fracture connections at the site can be summarized
610 as follows:

611 • $B1 - B2$ borehole pair is mainly connected through $B1 - 2$ and $B2 - 2$

612 • $B1 - B3$ borehole pair is mainly connected through the cluster that

27

613   consists of $B3-1$, $B3-2$, $B1-1$ and $B1-2$ fractures

614   • $B2-B3$ borehole pair is mainly connected through 2 independent
615   clusters. The first one consists of $B2-2$, $B3-1$ and $B3-2$, and the
616   second one consists of $B2-4$ and $B3-3$.

5. Comparison With Results From Flowmeter Tests and Ground-Penetrating Radar Data

619   Analysis of fracture connections on this field site have been also conducted
620 by *Le Borgne et al.* (2007), *Dorn et al.* (2012) and *Dorn et al.* (2013). *Le*
621 *Borgne et al.* (2007) used televiewer data together with cross-borehole single
622 packer testing and cross-borehole flowmeter testing at the site to characterize
623 fracture hydraulic connections. Comparison with our results demonstrates
624 that temperature based approach provides consistent results with very few
625 exceptions. Thus, flowmeter tests and packer tests both confirm that B2 well
626 is connected to B1 and B3 wells mostly through B2-2 fracture. The main
627 difference concerns to the connection of B2-4 fracture zone to B1 borehole,
628 which we find here to be poorly connected (Figure 9). *Le Borgne et al.* (2007)
629 found that, although the main head variation during single packer tests is
630 occurring in the B2-2 fracture zone in B2 when pumping in B1, the $B2-4$
631 fracture zone appears also to be connected to B1.

632   *Dorn et al.* (2012) used tracer test data combined with single-hole ground-
633 penetrating radar (GPR) data to characterize pattern of fractures that con-
634 tribute to tracer transport in between B1 and B2 wells. The images obtained
635 confirmed the existence of a network of connected fractures including the
636 B2-2, B2-4 and B1-4 fractures. However, fractures that contribute to tracer

28

637 transport are not necessarily those that provide the significant contribution
638 to flow (*Dorn et al.*, 2012). Furthermore, for some fracture patterns, our
639 conceptual approach introduces some constraints on fracture connections.
640 For instance, in our approach, the B2-4 fracture can not be connected to
641 any other fracture without being connected to the B1-4 fracture. A possible
642 solution to tackle the problem would be the use of more realistic fracture
643 geometry provided through geophysical data (*Dorn et al.*, 2012).

644 *Dorn et al.* (2013) used hydraulic, tracer, televiewer and GPR reflec-
645 tion data to generate stochastic 3-D discrete fracture models in the vicinity
646 of the B1 and B2 boreholes such that these fracture networks agree with
647 all available data. They also performed flow simulations on the proposed
648 discrete fracture networks in order to derive the effective transmissivity of
649 hydraulic connections between the boreholes. Their values of the effective
650 transmissivities varied in the range of $10^{-6} - 10^{-3}$ m^2/s that matches well
651 with our estimates. For the individual hydraulic connections, they found the
652 B1-4 - B2-2 fracture connection to be the most transmissive, and that B1-2
653 and B1-3 fractures are well connected to B2 borehole, which is in agreement
654 with our results in Figure 9. As expected, the fracture network geometry
655 inferred from GPR data is much more complex than the conceptualization
656 used in the present study. In particularly, we didn't include in our model
657 two fractures, intersected B2 borehole at 49 and 52 m depth (*Dorn et al.*,
658 2013). However, as flow prediction made by our flow model are reasonnable
659 and flow contributions of these fractures are negligible, we believe that these
660 simplifications not change a lot in terms of fracture network transmissivity.
661 This point emphasize that both methods are complementary: geometry can

29

662 be constrained from geophysical data, whereas hydraulic properties can be
663 inferred from flow tomography data.

6. Discussions and Conclusions

665 The temperature tomography approach (i.e. sequential borehole temper-
666 ature logging under cross-borehole flow conditions) has been proposed here
667 as a method to characterize the connectivity and transmissivity of preferen-
668 tial permeable flow paths in fractured aquifers. An inverse model framework
669 was developed to estimate log-transformed transmissivity values of hydrauli-
670 cally active fractures between and around borehole pairs. We first detect the
671 main permeable fractures through inversion of borehole temperature profiles
672 under pumping conditions. Then we apply a borehole-scale flow and tem-
673 perature model to produce flowmeter profiles by inversion of temperature
674 profiles. Finally we invert the obtained cross-borehole flowmeter profiles in
675 order to infer inter-borehole fracture connectivity and transmissivities.

676 The method proposed has been successfully applied to temperature to-
677 mography data obtained from a fractured rock aquifer. The results of ap-
678 plication of the proposed approach to the Stang Er Brune experimental site
679 (Ploemeur) can be synthesized as follows:

680 • A general flow pattern for the experimental site is proposed based on
681 the analysis of borehole temperature profiles under ambient flow con-
682 ditions.

683 • The inversion of single-borehole flow and cross-borehole temperature
684 data is shown to allow the detection of the main fractures at the site
685 and to image their hydraulic properties.

30

686 • In some cases of multi-fracture connections it appears difficult to pro-
687 pose a simple conceptual model of flow and connectivity.

688 These first applications are encouraging in that, even though the fracture
689 network geometry has been simplified, the estimates of fracture connectivity
690 and hydraulic properties are generally consistent with other data sets avail-
691 able on this site. In the future, tracer experiments and geophysical surveys
692 (*Dorn et al.*, 2012) may be coupled with temperature data to assess the over-
693 all fracture network geometry and its hydraulic properties. Furthermore, a
694 possible extension of this inverse approach could exploit simultaneous joint
695 inversion of multiple pumping tests with more than two boreholes to identify
696 and characterize a connected fracture cluster all over the site.

697 The temperature tomography approach proposed in this study has some
698 limitations. First, the method is not sufficiently sensitive to identify all
699 flowing fractures in a given borehole and only allows the detection of the
700 most transmissive fractures. Second, the capacity of this approach is lim-
701 ited when cross-borehole pumping induces similar hydraulic head variations
702 within flow paths connecting borehole pair. In this case, the resulting ve-
703 locity in the concerned section of observation borehole is close to zero and
704 uncertainty about corresponding parameter drastically increases. Third, as
705 the approach is based on indirect measurements of temperature, in order
706 to obtain detectable temperature variations, significant flow velocities are
707 required to apply successfully the methodology proposed (*Klepikova et al.*,
708 2011). Finally, it also requires the temperature to change with depth.

709 Although there are some limitations, we argue that the temperature to-
710 mography method is a promising alternative to hydraulic tomography tests

31

[711] that require the use of straddle packers. In particular, the temperature to-
[712] mography approach was found to be clearly useful for fractured rock aquifers
[713] as Ploemeur field site (*Le Borgne et al.*, 2006, 2007). The method is also
[714] likely to be applicable to field sites with significant flow velocities such as
[715] karst aquifers (e.g. *Chatelier et al.*, 2011). Another interesting question of
[716] investigation is whether the method proposed could be used to characterize
[717] alluvial aquifers. However, getting necessary information in such type of en-
[718] vironment will probably require more detailed temperature measurements.
[719] Further work is required to answer this question.

7. Acknowledgments

References

[726] Anderson, M. P. (2005), Heat as a ground water tracer, *Ground Water*, *43*(6),
[727] 951–968.

[728] Barton, C. A. and Zoback, M. D. and Moos, D. (1995), Fluid flow along
[729] potentially active faults in crystalline rock, *Geology, 23*(8).

[730] Barton, C. A. and M. D. Zoback (1992), Self-Similar Distribution and Prop-
[731] erties of Macroscopic Fractures at Depth in Crystalline Rock in the Cajon

32

732 Pass Scientific Drill Hole, *Journal of Geophysical Research, 97*(B4), 5181–
733 5200.

734 Bense, V. F., Person, M. A., Chaudhary, K., You, Y., Cremer, N., and S.
735 Simon (2008), Thermal anomalies indicate preferential flow along faults
736 in unconsolidated sedimentary aquifers, *Geophysical Research Letters,*
737 *35*(24), L24406, doi:10.1029/2008GL036017.

738 Berg, S.J., and W.A. Illman (2013), Field Study of Subsurface Heterogeneity
739 with Steady-State Hydraulic Tomography, *Ground Water, 51*(1), 29–40.

740 Berkowitz B. (2002), Characterizing flow and transport in fractured geolog-
741 ical media: A review, *Advances in Water Resources, 25*, 861–884.

742 Bidaux, P., and C. Drogue (1993), Calculation of low-range flow velocities
743 in fractured carbonate media from borehole hydrochemical logging data
744 comparison with thermometric results, *Ground Water, 31*(1), 19–26.

745 Brauchler, R., R. Liedl and P. Dietrich (2003), A travel time based hy-
746 draulic tomographic approach, *Water Resource Research, 39*(12), 1370,
747 doi10.1029/2003WR002262.

748 Bredehoeft, J. H., and I. S. Papadopulos (1965), Rates of vertical groundwa-
749 ter movement estimated from the Earth's thermal profile, *Water Resource*
750 *Research, 1*, 325–328.

751 Chatelier, M., S. Ruelleu, O. Bour, G. Porel, and F. Delay (2011), Combined
752 fluid temperature and flow logging for the characterization of hydraulic
753 structure in a fractured karst aquifer, *Journal of Hydrology, 400*, 377-386.

33

754 Deming D. (1993), Regional permeability estimates from investigations of
755 coupled heat and groundwater flow, North Slope of Alaska, *Journal of*
756 *Geophysical Research*, *98*, 16271–16286.

757 Dorn C., N. Linde, T. Le Borgne, O. Bour, and M. Klepikova (2012), In-
758 ferring transport characteristics in a fractured rock aquifer by combining
759 single-hole GPR reflection monitoring and tracer test data, *Water Resource*
760 *Research*, *48*, W11521, doi10.1029/2011WR011739.

761 Dorn C., N. Linde, T. Le Borgne, O. Bour, and J.-R. de Dreuzy
762 (2013), Conditioning of stochastic 3-D fracture networks to hydrolog-
763 ical and geophysical data, *Advances in Water Resources*, *62*, 79-89,
764 doi10.1016/j.advwatres.2013.10.005.

765 Elci, A., Molz, F. J. and Waldrop, W. R. (2001), Implications of Observed
766 and Simulated Ambient Flow in Monitoring Wells, *Ground Water*, *39*,
767 853862. doi10.1111/j.1745-6584.2001.tb02473.x.

768 Ferguson G. (2006), Perturbation of ground surface temperature reconstruc-
769 tions by groundwater flow, *Geophysical Research Letters, 33*, L13708,
770 doi10.1029/2006GL026634.

771 Flynn T. (1985), *Water temperature as a groundwater tracer in fractured*
772 *rock*, M.S. thesis, Univ. of Arizona, Tucson.

773 Freifeld, B. M., S. Finsterle, T. C. Onstott, P. Toole, and L. M. Pratt
774 (2008), Ground surface temperature reconstructions: Using in situ es-
775 timates for thermal conductivity acquired with a fiber-optic distributed

776   thermal perturbation sensor, *Geophysical Research Letters, 35*, L14309,
777   doi10.1029/2008GL034762.

778 Gallagher, K., Bodin, T., Sambridge, M., Weiss, D., Kylander, M., Large,
779   D. (2011), Inference of abrupt changes in noisy geochemical records using
780   transdimensional changepoint models, *Earth and Planetary Science Let-*
781   *ters, 311*(1), 182–194, doi10.1016/j.epsl.2011.09.015.

782 Garibaldi, C., Guillou-Frottier, L., Lardeaux, J. M., Bonte, D., Lopez, S.,
783   Bouchot, V. and Ledru, P. (2010), Thermal anomalies and geological struc-
784   tures in the Provence basin: Implications for hydrothermal circulations at
785   depth, *Bulletin de la Société Géologique de France, 181*(4), 363-376.

786 Ge, S. M. (1998), Estimation of groundwater velocity in localized fracture
787   zones from well temperature profiles, *Journal of Volcanology and Geother-*
788   *mal Research, 84*(1–2), 93-101.

789 Genter, A., Castaing, C., Dezayes, C., Tenzer, H., Traineau, H., villemin, T.
790   (1997), Comparative analysis of direct (core) and indirect (borehole imag-
791   ing tools) collection of fracture data in the Hot Dry rock soultz reservoir
792   (France), *J. Geophys. Res., 102*(B7), 1541915431.

793 Hess, A. E. (1986), Identifying hydraulically conductive fractures with a slow
794   velocity borehole flowmeter, *Canadian Geotechnical Journal, 23*, 69–78.

795 Illman, W. A.,X. Liu,S. Takeuchi, T.-C. J. Yeh, K. Ando, and H. Sae-
796   gusa (2009), Hydraulic tomography in fractured granite: Mizunami Un-
797   derground Research site, Japan, *Water Resource Research, 45*, W01406,
798   doi10.1029/2007WR006715.

35

799 Incropera and DeWitt (1996), Fundamentals of heat and mass transfer, 4th
800 ed., *New York: Wiley*.

801 Klepikova, M. V., T. Le Borgne., O. Bour, P. Davy (2011), A methodology for
802 using temperature-depth profiles under ambient, single and cross-borehole
803 pumping conditions to estimate fracture hydraulic properties, *Journal of*
804 *Hydrology*, *407*(1-4), 145–152, doi10.1016/j.jhydrol.2011.07.018.

805 Klepikova, M. V., T. Le Borgne., O. Bour, J.-R. de Dreuzy, Inverse mod-
806 elling of flow tomography experiments in fractured media, *Water Resource*
807 *Research*, *49*(11), 7255–7265, doi10.1002/2013WR013722.

808 Keys, W. S. (1979), Borehole geophysics in igneous and metamorphic rocks,
809 *Trans. SPWLA Annual Logging Syrup., 20th, 407*, 1-26.

810 Lagarias, J.C., J. A. Reeds, M. H. Wright, and P. E. Wright (1998), Conver-
811 gence Properties of the Nelder-Mead Simplex Method in Low Dimensions,
812 *SIAM Journal of Optimization*, *9*(1), 112–147.

813 Leaf, A. T., D. J. Hart, J. M. Bahr (2012), Active thermal tracer tests
814 for improved hydrostratigraphic characterization, *Ground Water*, *50*(5),
815 doi10.1111/j.1745-6584.2012.00913.x.

816 Jolivet, J., G. Bienfait, J. L. Vigneresse, and M. Cuney (1988), Heat flow
817 and heat production in Brittany (Western France), *Tectonophysics, 159*,
818 61-72.

819 Le Borgne, T., Paillet, F.L., Bour, O., Caudal, J.-P. (2006), Cross-borehole

36

820 flowmeter tests for transient heads in heterogeneous aquifers, *Ground Wa-*
821 *ter*, *44*, doi10.1111/j.1745-6584.2005.00150.x.

822 Le Borgne, T., O. Bour, M.S. Riley, P. Gouze, P.A. Pezard, A. Belghoul,
823 G. Lods, R. Le Provost, R. B. Gresswell, P. A. Ellis, E. Isakov, and B. J.
824 Last (2007), Comparison of alternative methodologies for identifying and
825 characterizing preferential flow paths in heterogeneous aquifers, *Journal of*
826 *Hydrology*, *345*(3-4), 134–148, doi10.1016/j.jhydro1.2007.07.007.

827 Mwenifumbo, C. J. (1993), Temperature logging in mineral exploration,
828 *Journal of Applied Geophysics*, *30*, 297–313.

829 Newhouse, M. W., J. A. Izbicki and G. A. Smith (2005), TComparison of
830 velocity-log data collected using impeller and electromagnetic flowmeters,
831 *Ground Water*, *43*, 434-438.

832 Paillet, F. L. (1998), Flow modeling and permeability estimation using bore-
833 hole flow logs in heterogeneous fractured formations, *Water Resource Re-*
834 *search*, *34*(5), 997–1010.

835 Paillet, F. L. (2000), A field technique for estimating aquifer parameters
836 using flow log data, *Ground Water*, *38*(4), 510–521.

837 Paillet, F. L. (2004), Borehole flowmeter applications in irregular and large-
838 diameter boreholes, *Journal of Applied Geophysics*, *55*, 39–59.

839 Paillet, F. L., J. H. Williams, J. Urik, J. Lukes, M. Kobr and S. Mares
840 (2012), Cross-borehole flow analysis to characterize fracture connections

37

841   in the Melechov Granite, Bohemian-Moravian Highland, Czech Republic,

842   *Hydrogeology Journal*, *20*(1), 143–154, doi10.1007/s10040-011-0787-1.

843 Pehme, P.E., B.L. Parker, J.A. Cherry, and J.P. Greenhouse (2010), Im-

844   proved resolution of ambient flow through fractured rock with temperature

845   logs, *Ground Water*, *48*(2), 191-205.

846 Pehme, P.E., B.L. Parker, J.A. Cherry, J.W. Molson and J.P. Greenhouse

847   (2013), Enhanced detection of hydraulically active fractures by temper-

848   ature profiling in lined heated bedrock boreholes, *Journal of Hydrology*,

849   *48*(0), 1–15.

850 Perry, H. K. C., C. Jaupart, J.-C. Mareschal, and G. Bienfait (2006), Crustal

851   heat production in the Superior Province, Canadian Shield, and in North

852   America inferred from heat flow data, *J. Geophys. Res.*, 111, B04401,

853   doi10.1029/2005JB003893.

854 Quinn, P.M., J.A. Cherry, B.L. Parker (2011), Quantification of non-Darcian

855   flow observed during packer testing in fractured rock, *Water Resource Re-*

856   *source*, *47*(9), W09533, doi10.1029/2010WR009681.

857 Read, T., O. Bour, V. F. Bense, T. Le Borgne, P. Goderniaux, M. Klepikova,

858   R. Hochreutener, N. Lavenant and V. Boschero (2013), Characterizing

859   groundwater flow and heat transport in fractured rock using fiber-optic dis-

860   tributed temperature sensing, *Geophysical Research Letters*, *40*(10), 2055–

861   2059, doi10.1002/grl.50397.

862 Reiter, M. (2001), Using precision temperature logs to estimate horizon-

38

863   tal and vertical groundwater flow components, *Water Resource Research*,
864   *37*(3), 663–674.

865   Saar, M. O. (2011), Review: Geothermal heat as a tracer of large-scale
866   groundwater flow and as a means to determine permeability field, *Hy-*
867   *drogeology Journal*, *19*, 31–52.

868   Sawdey, J.R., and A.S. Reeve (2012), Automated inverse computer model-
869   ing of borehole flow data in heterogeneous aquifers, *Computers and Geo-*
870   *sciences*, *46*, 219–228.

871   Silliman, S. and Robinson, R. (1989), Identifying Fracture Interconnections
872   Between Boreholes Using Natural Temperature Profiling: I. Conceptual
873   Basis, *Ground Water*, *27*, 393402, doi10.1111/j.1745-6584.1989.tb00463.x.

874   Shapiro, A. M. and Hsieh, P. A.(1998), How good are estimates of transmis-
875   sivity from slug tests in fractured rock?, *Ground Water*, *36*, 37–48.

876   Sharmeen, R., W. A. Illman, S. J. Berg, T.-C. J. Yeh, Y.-J. Park, E. A. Su-
877   dicky, and K. Ando (2012), Transient hydraulic tomography in a fractured
878   dolostone: Laboratory rock block experiments, *Water Resource Resource*,
879   *48*, W10532, doi10.1029/2012WR012216.

880   Tarantola, A. (2004), Inverse Problem Theory and Model Parameter Esti-
881   mation, *SIAM*.

882   Wagner, V. , Li, T., Bayer, P. and Leven, C., Dietrich, P. and Blum, P.
883   (2013), Thermal tracer testing in a sedimentary aquifer: field experiment

39

884 (Lauswiesen, Germany) and numerical simulation, *Hydrogeology Journal*,

885 doi10.1007/s10040-013-1059-z.

886 Williams, G. R., G, Brown, W. Hawthorne, A. H. Hartog and P. C. Waite

887 (2000), Distributed temperature sensing (DTS) to characterize the per-

888 formance of producing oil wells, *Proc. SPIE, Industrial Sensing Systems*,

889 doihttp://dx.doi.org/10.1117/12.411726.

890 Yeh T. C. Jim and S. Liu (2000), Hydraulic tomography: Development of a

891 new aquifer test method, *Water Resources Research*, 36(8), 2095–2105.

40
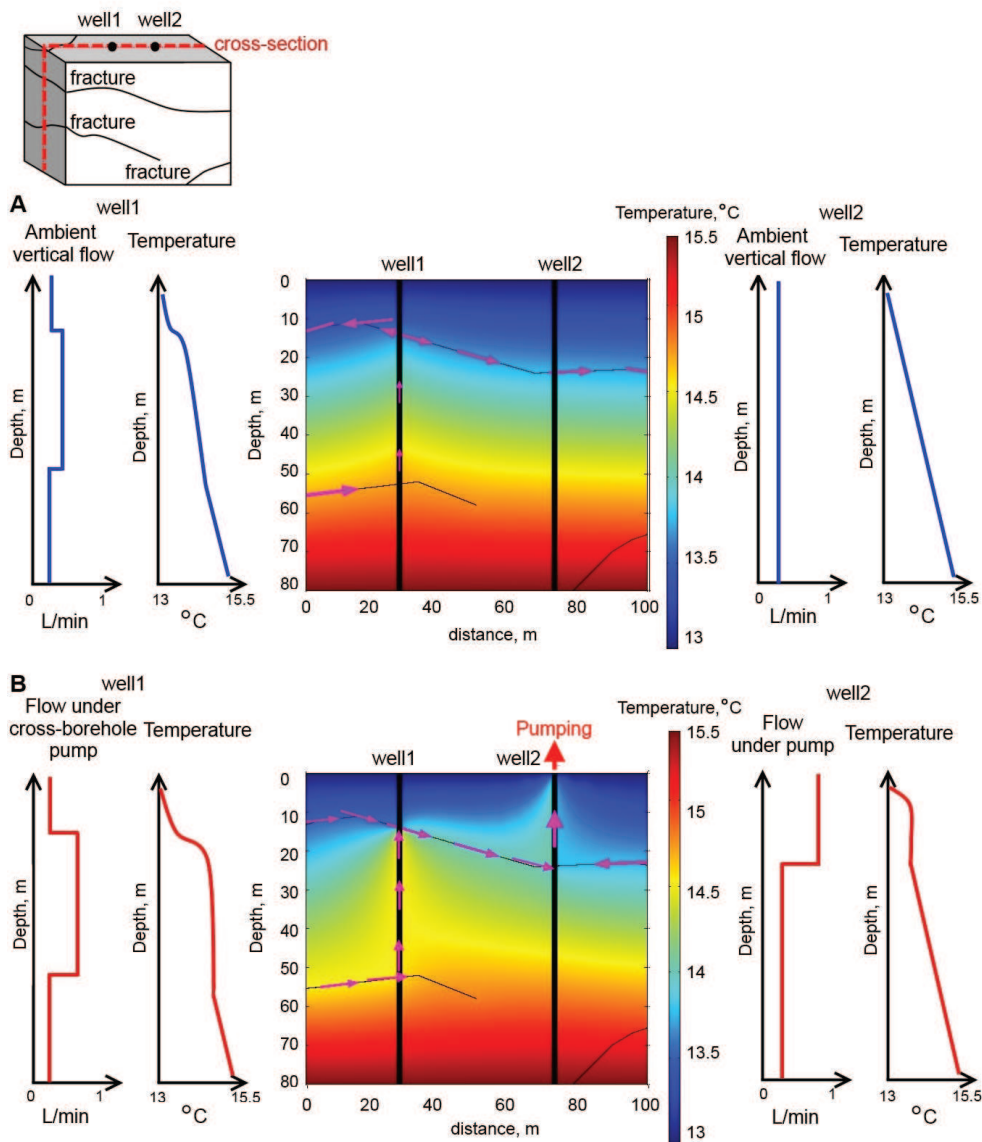
Figure 1: Illustration of a typical groundwater flow and temperature fields for a pair of boreholes connected by one main flow path and intersected by one disconnected fracture each borehole under ambient (A) and pumping (B) flow conditions. The velocity field and temperature field are computed using 2D model.

41
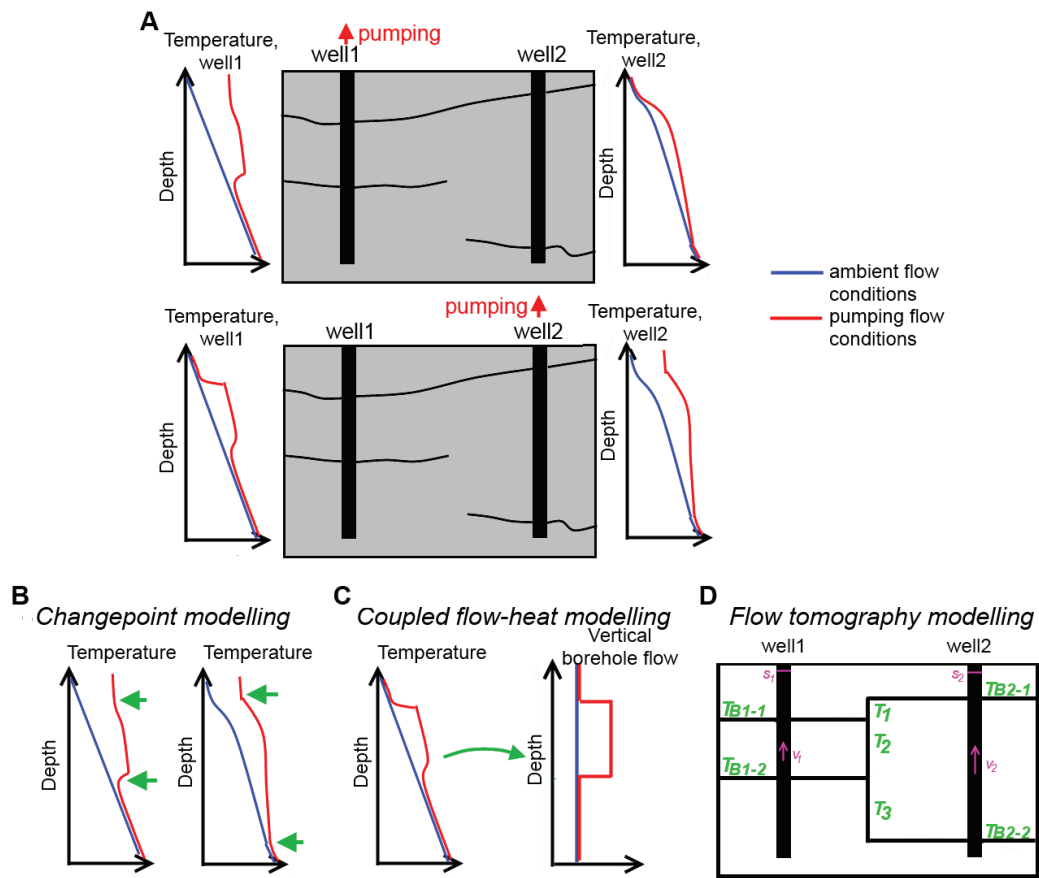
Figure 2: Illustration of the temperature tomography field method conducted in between two boreholes connected by one fracture and intersected by two disconnected fractures (a). Temperature profiles measured under ambient and pumping flow conditions are shown by blue and red correspondingly. Illustration of processing steps of an inverse framework for interpretation of such a data set: (b) automatic fracture detection by applying changepoint modelling; (c) inversion of temperature profiles under ambient, single and cross-borehole flow conditions to derive flow profiles; (d) estimation of fracture hydraulic properties and connectivity between and around a borehole pair by applying flow tomography modelling.

42
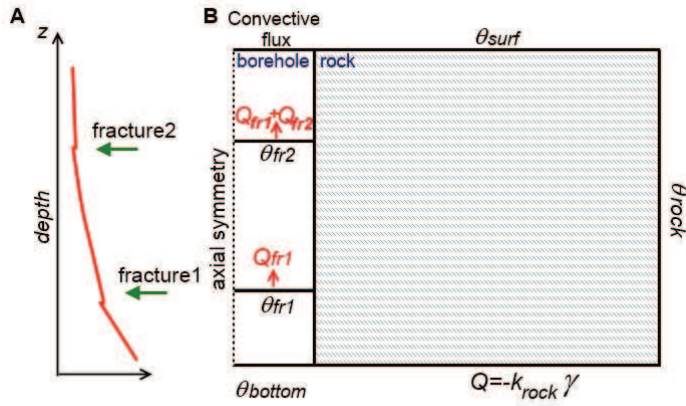
Figure 3: Illustration of the flow and temperature propagation simulation in a borehole. Borehole temperature profile with inferred fracture positions (A) and corresponding heat transfer model boundary conditions (B). We consider the heat diffusion and advection of heat with a constant vertical laminar flow in the borehole and the heat diffusion in the surrounding rock matrix. For each borehole section we impose the borehole flow as the sum of all fractures inflows and outflows (Q_{fr}) below the modeled section (shown by red).

43
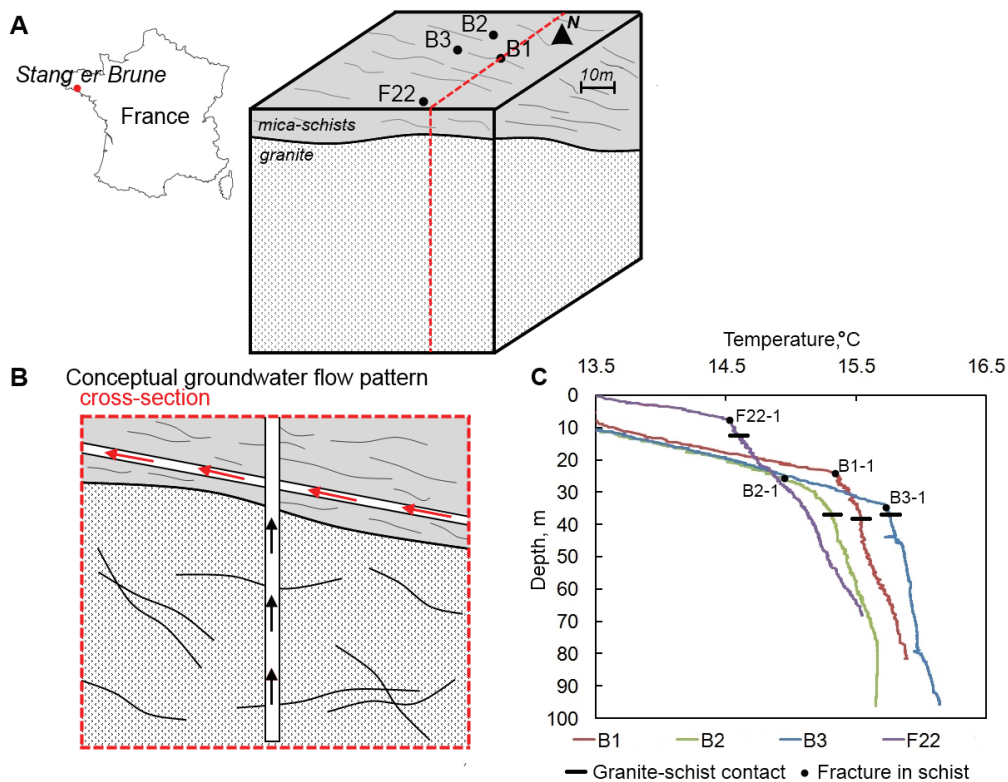
Figure 4: A. Location of the Stang-er-Brune study site, boreholes array configuration and geology of the site. B. Conceptual hydrothermal setting: temperature profile affected by groundwater flow of warmer origin, by localized flow of warmer or cooler origin in narrow fractures and by vertical flow in the borehole itself. C. Temperature profiles measured at the site under the ambient flow conditions.

44
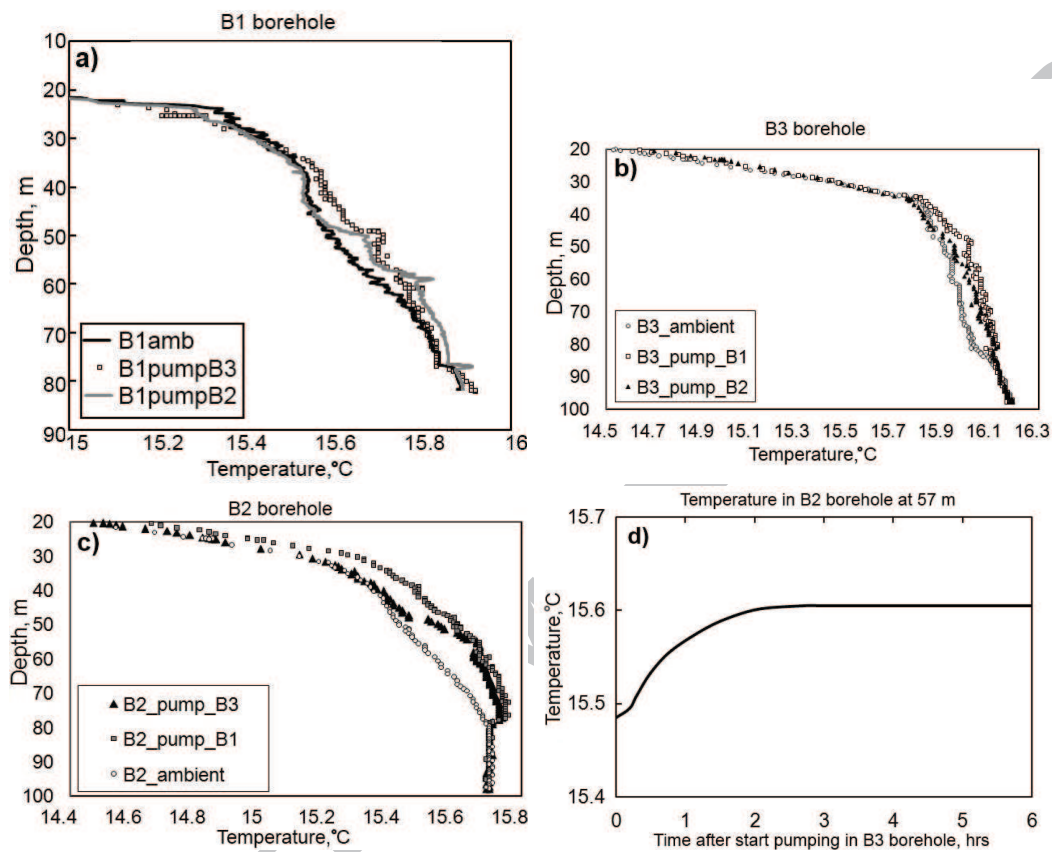
Figure 5: Temperature tomography experiment. Steady-state temperature profiles measured in B1 well when pumping in B2 and B3 wells (a). Steady-state temperature profiles measured in B2 well when pumping in B1 and B3 wells (b). Steady-state temperature profiles measured in B3 well when pumping in B1 and B2 wells (c). Example of temporal evolution of temperature in B2 at 57 m depth (d).

45
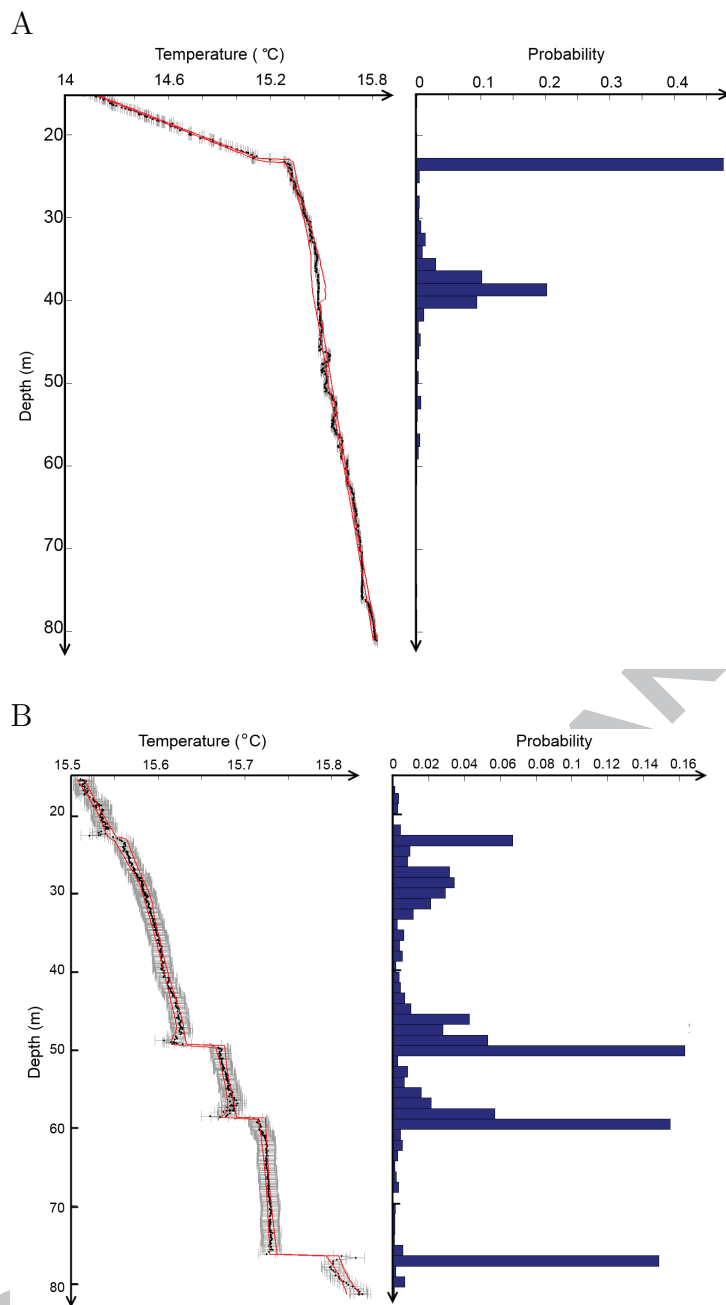
Figure 6: Inferred changepoint models for the temperature profiles measured in B1 borehole under ambient (A) and pumping (B) flow conditions, while pumping at the top of B1 with a pumping rate $Q = 20 \ l/min$. The solid red line is the inferred function (relative to the down axis), and the solid black line represents the probability of a changepoint (relative to the upper axis). The error bars are drawn using the mean value of the noise variances for each data set (relative to the down axis). The most probable inferred numbers of changepoints are 2 and 4 respectively.

46
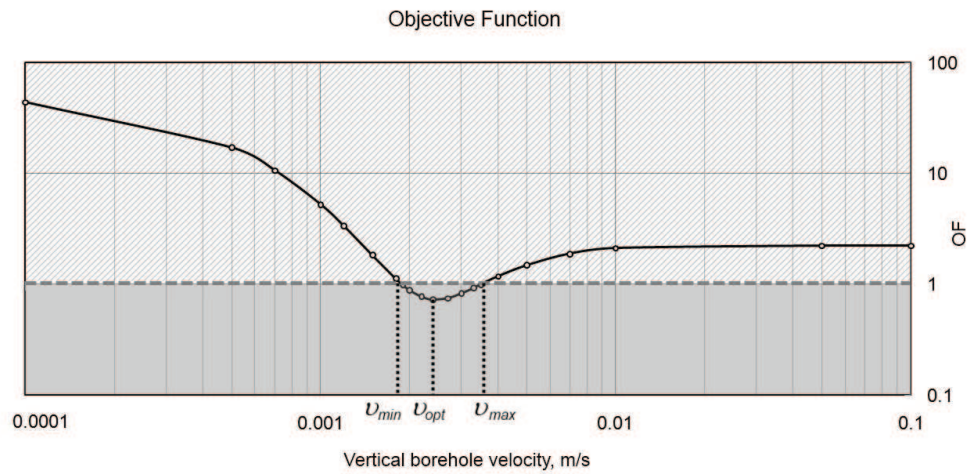
Figure 7: Example of the objective function versus the vertical borehole flow velocity. The minima of the objective function corresponds to the optimal flow velocity (v_{opt}), and all the solutions in the range (v_{min}, v_{max}) are acceptable.

47
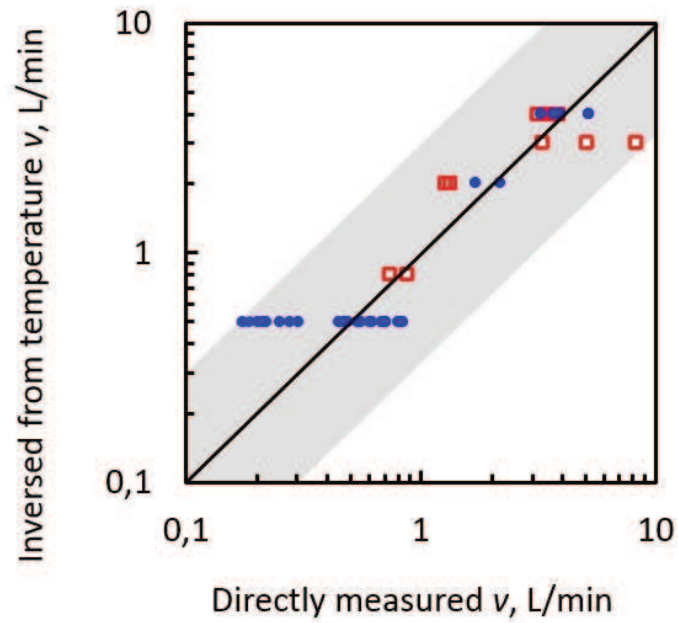
Figure 8: Comparison between flowmeter measurements and velocity values inverted from temperature measurements. Blue markers correspond to ambient flow conditions, while red markers correspond to cross-borehole pumping conditions. Note, that this plot also demonstrates the variability of the flow measurements inside borehole sections due to the tool error and/or variations in borehole diameter.

48
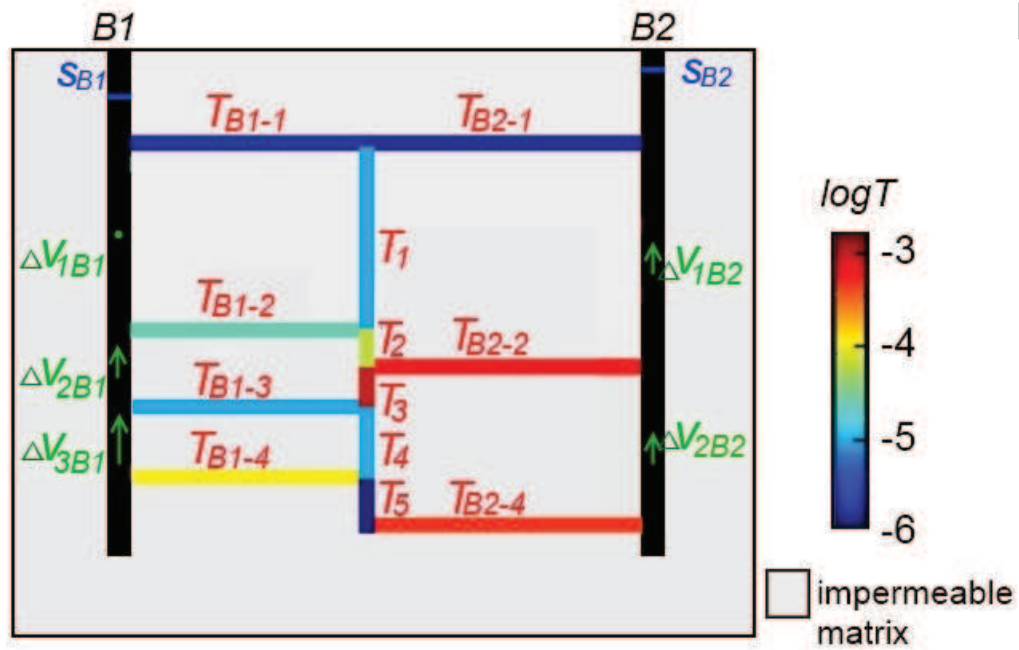
Figure 9: Inferred fracture transmissivities (T) and connectivities between and around B1-B2 borehole pair. Observation well drawdowns during cross-borehole pumping s are shown by blue lines. Variations of vertical velocities during cross-borehole pumping Δv in observation boreholes are shown by green arrows.

49
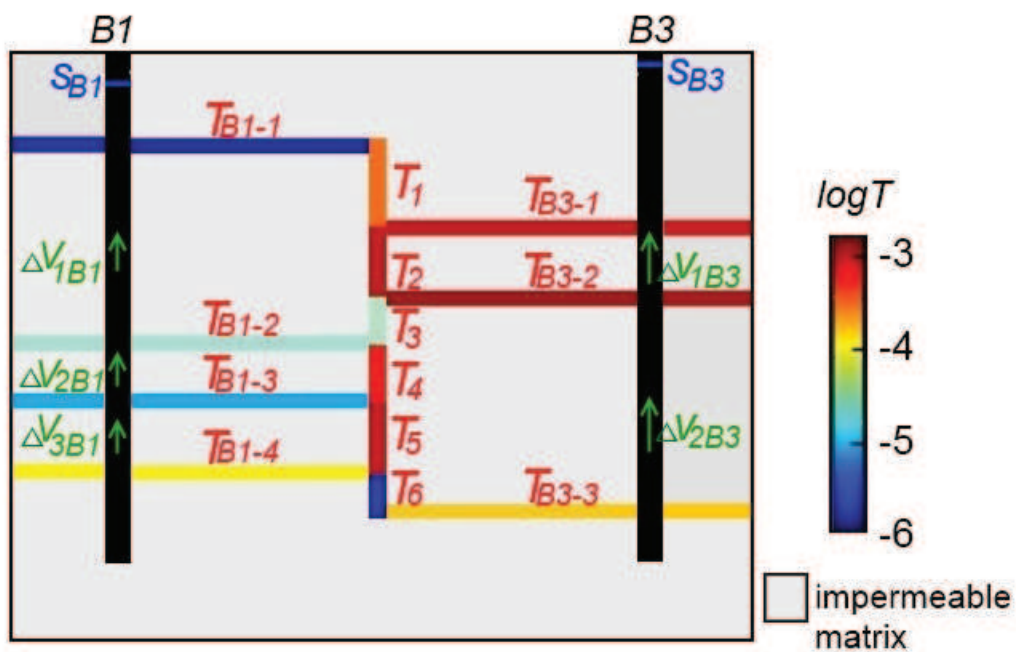
Figure 10: Inferred fracture transmissivities (T) and connectivities between and around B3-B1 borehole pair. Observation well drawdowns during cross-borehole pumping s are shown by blue lines. Variations of vertical velocities during cross-borehole pumping Δv in observation boreholes are shown by green arrows.

50
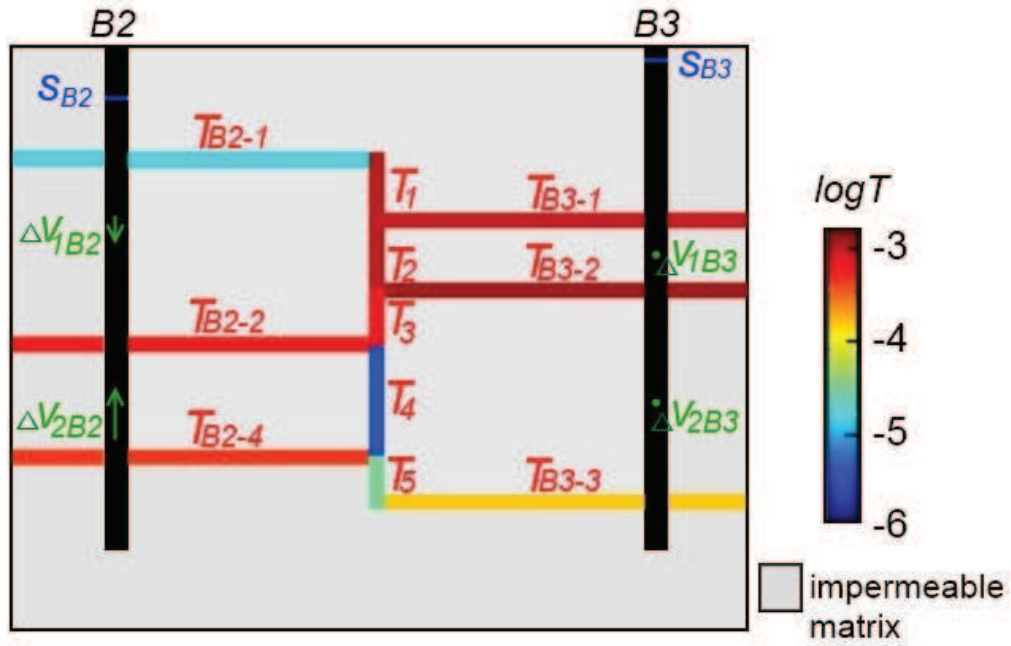
Figure 11: Inferred fracture transmissivities (T) and connectivities between and around B2-B3 borehole pair. Observation well drawdowns during cross-borehole pumping s are shown by blue lines. Variations of vertical velocities during cross-borehole pumping Δv in observation boreholes are shown by green arrows.

51

Table 1: Inferred fracture transmissivities. We utilized ambient and steady pumping single-borehole flow profiles and drawdowms in order to infer local fracture transmissivities and cross-borehole flow profiles and drawdowns were used for inversion of connected fracture transmissivities.

Scale	Well	Data used for inversion	Fracture	T, m^2/s
Transmissivities of the main fractures in the near field	B1	1 drawdown, 3 velocities	T_{B1-1}	$2 \cdot 10^{-6}$
			T_{B1-2}	$4 \cdot 10^{-5}$
			T_{B1-3}	$1.3 \cdot 10^{-5}$
			T_{B1-4}	$1.6 \cdot 10^{-4}$
	B2	1 drawdowns, 2 velocities	T_{B2-1}	$2 \cdot 10^{-6}$
			T_{B2-2}	$8 \cdot 10^{-4}$
			T_{B2-4}	$5 \cdot 10^{-4}$
	B3	1 drawdowns, 2 velocities	T_{B3-1}	$8 \cdot 10^{-4}$
			T_{B3-2}	$1.3 \cdot 10^{-3}$
			T_{B3-3}	$1.6 \cdot 10^{-4}$
Transmissivities of the main connected fractures	B1-B2	2 drawdowns, 5 velocities	T_1	$1.3 \cdot 10^{-5}$
			T_2	$8 \cdot 10^{-5}$
			T_3	$1.6 \cdot 10^{-3}$
			T_4	$1.3 \cdot 10^{-5}$
			T_5	$1.6 \cdot 10^{-6}$
	B1-B3	2 drawdowns, 5 velocities	T_1	$3.2 \cdot 10^{-4}$
			T_2	$1 \cdot 10^{-3}$
			T_3	$3.2 \cdot 10^{-5}$
			T_4	$5 \cdot 10^{-4}$
			T_5	$1 \cdot 10^{-3}$
			T_6	$2.5 \cdot 10^{-6}$
	B2-B3	2 drawdown, 4 velocities	T_1	$1 \cdot 10^{-3}$
			T_2	$1 \cdot 10^{-3}$
			T_3	$6.3 \cdot 10^{-4}$
			T_4	$4 \cdot 10^{-6}$
			T_5	$3.2 \cdot 10^{-5}$

Table 2: Comparison of flow tomography data, inverted from temperature measurements, with numerical solutions that best matches the data. Flow tomography data include drawdowns s and variations of vertical borehole flow velocities Δv during cross-borehole pumping in observation boreholes. The values of fracture transmissivities that yield the best match to the data are presented in Figure 9 for B1-B2 borehole pair, in Figure 10 for B1-B3 borehole pair and in Figure 11 for B2-B3 borehole pair. The corresponding data errors are $\sigma_v = 1\ mm/s$ and $\sigma_s = 2\ cm$ for flow and drawdown respectively.

Borehole pair	Observation	Flow tomography data	Best match to the data	OF value
B1-B2	s_{B1}, cm	34	29	
	s_{B2}, cm	15	15	
	Δv_{1B1}, mm/s	0	0	
	Δv_{2B1}, mm/s	1	1	3.7
	Δv_{3B1}, mm/s	3	1.3	
	Δv_{1B2}, mm/s	1.1	0.5	
	Δv_{2B2}, mm/s	1.1	1.3	
B1-B3	s_{B1}, cm	19	16	
	s_{B3}, cm	2	7	
	Δv_{1B1}, mm/s	1.4	0	
	Δv_{2B1}, mm/s	1.4	0	6.35
	Δv_{3B1}, mm/s	1.4	0.5	
	Δv_{1B3}, mm/s	2.8	0.5	
	Δv_{2B3}, mm/s	2.8	3.4	
B2-B3	s_{B2}, cm	14	14.9	
	s_{B3}, cm	18	16	
	Δv_{1B2}, mm/s	-0.8	0	1.05
	Δv_{2B2}, mm/s	1.4	1	
	Δv_{1B3}, mm/s	0	-1	
	Δv_{2B3}, mm/s	0	0	

53

Highlights

- Temperature tomography is proposed as a new method for characterizing fractured media
- We propose an inverse multi-step framework to interpret borehole temperature profiles
- We automatically detect permeable fractures from borehole temperature profiles
- We produce flow profiles by inversion of temperature profiles
- We inverse flow profiles to infer fracture transmissivities and connectivity